Pt Sub-Monolayer on Au: System Stability and Insights into Platinum Electrochemical Dissolution

Serhiy Cherevko,[a,b,z] Gareth P. Keeley,[a] Nadiia Kulyk,[a] and Karl J. J. Mayrhofer[a,b,*,z]

[a]*Department of Interface Chemistry and Surface Engineering, Max-Planck-Institut für Eisenforschung GmbH, 40237 Düsseldorf, Germany*
[b]*Forschungszentrum Jülich, "Helmholtz-Institut Erlangen-Nürnberg" (IEK11), 91052 Erlangen, Germany*

Platinum is the best single element oxygen reduction reaction electrocatalyst. In recent years, several advanced catalysts have been suggested. One of them is the so-called "*platinum monolayer electrocatalyst*". In this work we demonstrate the potential- and time-resolved dissolution characteristics of such sub-monolayer platinum supported on gold in potentiodynamic and potentiostatic regimes. It is shown that the as-prepared Pt@Au is not stable, but rather shows significant dissolution of both Pt and Au similar to the pure elements. Potential-resolved dissolution profiles reveal that anodic dissolution scales with Pt coverage, while cathodic dissolution and quasi-steady-state dissolution are Pt coverage independent. This implies a significantly higher Pt coverage normalized dissolution of Pt@Au, viz. a factor of four higher dissolution amounts for Pt coverage of 0.25. The onsets of Pt and Au dissolution are also comparable to the pure elements. Only after intermixing during potential cycling does the system become somewhat stabilized. The onset of Pt transient anodic dissolution shifts to more positive values. The data obtained in the current work provide new insights into the mechanism of platinum dissolution. It also aids the understanding of the previously observed effect of stabilization of Pt catalysts by addition of Au, and will therefore guide future developments for improving catalyst performance.

Manuscript submitted December 9, 2015; revised manuscript received December 22, 2015. Published January 6, 2016.

Degradation of cathode catalysts in corrosive acidic environment is one of the major obstacles hindering the commercialization of low-temperature proton exchange membrane fuel cells (PEMFCs).[1–6] The high price and low abundance of Pt, the state of the art oxygen reduction reaction (ORR) catalyst, aggravate the issue of degradation. One of the suggested mitigation strategies is the utilization of Pt@M (Pt – shell, M - core) core/shell ORR catalysts with M usually Pd, Au, Ir, and other noble metals or first-row transition metals, aiming at improved activity and stability while reducing Pt content at the same time.[7,8]

Due to enhanced Pt mass- and surface-area-normalized activity,[9–13] typical loadings of Pt in such catalysts can be significantly lower than those traditionally employed in commercial Pt/C-based catalysts. At the same time catalysts are supposed to have superior stability based on accelerated degradation tests, typically performed under rather mild conditions in half-cell rotating disc electrode investigations.[8,14–16] In contrast, however, data on PEMFC performance with core/shell catalysts typically indicate quite low activity, most likely due to catalyst instability.[17]

This is not surprising, considering the degradation of standard, pure Pt/C PEMFC cathode catalysts under various relevant conditions.[1–5] Particularly, the importance of the applied potential in relation to the quasi-steady-state and transient dissolution of Pt/C and polycrystalline Pt (Pt-poly) have been extensively discussed,[18–22] and the significant effect of short time excursions to strongly anodic and cathodic potentials on catalyst stability has been demonstrated (see Table I in Ref. 18). In order to clarify if indeed Pt can be stabilized against dissolution by Au, and to improve our understanding of the involved processes, in the current work a supposedly more stable Au-supported Pt sub-monolayer (Pt@Au) system is investigated using a scanning flow cell inductively coupled plasma mass-spectrometry (SFC-ICP-MS) setup, described in more detail in our previous works.[23,24]

Experimental

Two electrochemical setups were utilized in the current work. The first setup (Setup I) was based on a conventional three-electrode one-compartment electrochemical cell made of glass. This setup was used for underpotential deposition of copper (Cu_{UPD}). The second setup (Setup II), composed of a scanning flow cell (SFC) and an inductively coupled plasma mass-spectrometer (ICP-MS), was utilized in Cu, Pt, and Au dissolution studies.

Pt (99.99%) and Au (99.99%) foils were purchased from MaTecK, Germany. Prior to electrochemical experiments the foils were polished in 0.3 μm Al_2O_3 slurry followed by extensive washing in ultrapure water (PureLab Plus system, Elga, 18 MΩ, TOC < 3 ppb) and drying in a flow of argon. Afterwards, foils were electrochemically cleaned/activated (either using Setup I or II) applying 30 cycles up to 1.5 V_{RHE} (potential against the reversible hydrogen electrode) and 1.8 V_{RHE} at 200 mV s^{-1} on Pt and Au, respectively. The same saturated Ag/AgCl electrode and two graphite rods of different diameter and length were used as the reference and counter electrodes in the setups. The 0.1 M H_2SO_4 electrolytes were freshly prepared from Suprapur 96% sulfuric acid (Merck, Germany) by dilution in ultrapure water. This electrolyte was used in Setup I for cleaning/activation of the Au foil. Afterwards, the same volume of second electrolyte consisting of 0.1 M H_2SO_4 + 5 mM $CuSO_4 \cdot 5H_2O$ (98+%, Sigma-Aldrich) was added in the cell. Hence, the electrolyte used for Cu_{UPD} deposition was 0.1 M H_2SO_4 + 2.5 mM $CuSO_4 \cdot 5H_2O$. A sub-monolayer of Cu on Au was deposited by applying a potential of 0.4 V_{RHE} over time t = 2 min. Immediately after deposition, the electrode was removed from the electrolyte, washed in ultrapure water and dried in Ar. Afterwards the electrode was either moved to Setup II for dissolution studies or immersed in Pt deposition solution. The latter was composed of 0.1 M $HClO_4$ + 5 mM $H_2PtCl_6 \cdot 6H_2O$ (99.9%, Alfa Aesar). Pt was deposited on Au by galvanic replacement of the less noble Cu_{UPD}. Deposition time was t = 2 min. The as-prepared Pt@Au electrodes were used in dissolution studies using Setup II. The on-line detection of the concentration of dissolved Cu, Pt, and Au was performed by an ICP-MS (NexION 300X, Perkin Elmer). 10 mg L^{-1} ^{187}Re was used as an internal standard for both Pt and Au (mixing ratio 1 : 1). 10 mg L^{-1} ^{74}Ge was used as an internal standard for Cu. The 0.1 M $HClO_4$ electrolytes used in dissolution studies in Setup II were freshly prepared from Suprapur 70% $HClO_4$ (Merck, Germany) by dilution with ultrapure water. The electrolyte flow rate in the SFC was ca. 190 μL min^{-1}. The surface area of the working electrode exposed to the electrolyte was ca. 0.01 cm^{-2}. The flow rate and exposed area can be used to convert dissolved species concentration (μg L^{-1}) to dissolution rates (ng cm^{-2} s^{-1}). More details on the SFC-ICP-MS setup can be found in our previous works.[18,23] All electrolytes were saturated with Ar. All measurements were done at room temperature.

*Electrochemical Society Active Member.
[z]E-mail: cherevko@mpie.de; mayrhofer@mpie.de

Unless otherwise stated, electrical current and dissolution signal are normalized to the geometric surface area. The estimated roughness factor of the preconditioned Au and Pt foils was ca. 1.3. Error bars show the standard deviation of mean values obtained after at least three repetitions.

Results

Copper under-potential deposition and stripping on gold.—Sub-monolayer Pt on Au (Pt@Au) electrodes were prepared by a well-known galvanic replacement of a sacrificial layer of underpotentially deposited copper (Cu_{UPD}) with Pt.[25–27] A typical example of Cu cyclic voltammograms (CV) taken in a conventional three electrode cell with 0.1 M H_2SO_4 + 2.5 mM $CuSO_4$ Cu deposition solution is shown in Figure 1a. A Cu stripping linear sweep voltammogram (LSV) taken with the 0.1 M H_2SO_4 + 2.5 mM $CuSO_4$ Cu deposition solution is presented in dashed gray line in Figure 1b. Integrating the resulting current/time profile (after subtracting the background signal) yields a Cu stripping charge of ca. 370 μC cm^{-2}. The black solid line in the same figure presents the Cu stripping signal obtained using the Cu_{UPD}@Au electrode in the scanning flow cell (SFC) connected to an inductively coupled plasma mass spectrometer (SFC-ICP-MS) setup with the 0.1 M $HClO_4$ electrolyte. One can see that the stripping profile is different now, which can be attributed to the difference in electrolyte and/or to the amount of Cu presented (some removal of copper during washing, drying, and transfer of sample cannot be excluded). The Cu stripping charge was ca. 118 ± 25 μC cm^{-2}. For the latter, using Faraday's law of electrolysis and assuming the charge of dissolved species n = 1 or n = 2, we obtain values for the mass of dissolved copper of 60 ± 12 and 30 ± 6 ng cm^{-2}, respectively.

The Cu_{UPD}@Au electrodes were studied further using the SFC-ICP-MS setup. Figure 1c shows a typical Cu dissolution mass-spectrogram (dissolution profile) recorded by ICP-MS. It contains two characteristic peaks of Cu dissolution. The onset of the first (Cu_{A1}) peak always corresponded to the time for which the electrode is in contact with the electrolyte. This dissolution at open circuit potential (OCP) can be explained assuming corrosion of copper in the presence of oxygen in the electrolyte, the concentration of which may be significant at the time the SFC is approaching the electrode (even though an argon blanket is used). As soon as contact is established the amount of oxygen is limited by its diffusion through the tubes, cell, and silica ring and usually is low. Hence, dissolution ceases. The second (Cu_{A2}) dissolution peak coincides well with the onset of the anodic current increase shown in Figure 1b and can be attributed to electrochemical Cu stripping/dissolution. The average amount of Cu dissolved in the Cu_{A1} and Cu_{A2} peaks estimated by integration of the dissolution profiles over time was 17.6 ± 4.9 and 66.4 ± 8.1 ng cm^{-2}, respectively. The latter matches well with the calculated value assuming dissolution of monovalent copper ions. The total amount of dissolved copper was ca. 84 ± 12 ng cm^{-2}. The typical roughness factor (R_f) of polished and electrochemically activated Au was ca. 1.3. Hence, one calculates that the real-surface-area-normalized copper dissolution is ca. 65 ng cm^{-2}. Taking the weight an Au monolayer to be ca. 410 ng cm^{-2}[28–30] and the difference in the atomic weight between Au and copper, one would expect that the weight of copper monolayer on Au is approximately 130 ng cm^{-2} of real area. Combining all these values yields a total coverage of Cu on Au $\theta_{Cu} = 0.5$ (versus Au substrate) after deposition. The coverage of Cu dissolved in the peaks Cu_{A1} and Cu_{A2} is then $\theta_{Cu}(A1) = 0.1$ and $\theta_{Cu}(A2) = 0.4$, respectively.

Platinum shell deposition on gold by galvanic replacement of copper.—Pt sub-monolayer covered Au electrodes prepared by galvanic replacement of Cu_{UPD} with Pt were analyzed using the SFC-ICP-MS setup. As the charge of Pt ions in the employed salt was +4 one would expect that maximal coverage of Pt is two times lower than that of copper (assuming that each Cu atom provides two electrons to a Pt complex), i.e. $\theta_{Pt} = 0.25$. The weight of a Pt monolayer is ~400 ng cm^{-2}. Taking the R_f of the Au substrate to be 1.3 we find that the weight of Pt monolayer normalized to the geometric surface area is 520 ng cm^{-2}, while the total amount of Pt on Au at $\theta_{Pt} = 0.25$ is 130 ng cm^{-2} of the geometric surface area. This value is used in the estimation of electrode degradation described below. While also recorded, no change in the Cu blank signal was found when Pt@Au electrodes were used in the SFC-ICP-MS setup, indicating the complete displacement of Cu by Pt during Pt deposition.

Alternatively, θ_{Pt} can be estimated using the charge of the underpotentially deposited hydrogen (H_{UPD}) at Pt. This was done for activated Pt-poly and Pt@Au electrodes. Typical CVs for these two electrodes are shown in Figure S1 in the electronic supplementary information (ESI) file. The recorded CVs are obstructed in the region of cathodic potentials by reduction of oxygen passing through the silica ring of the

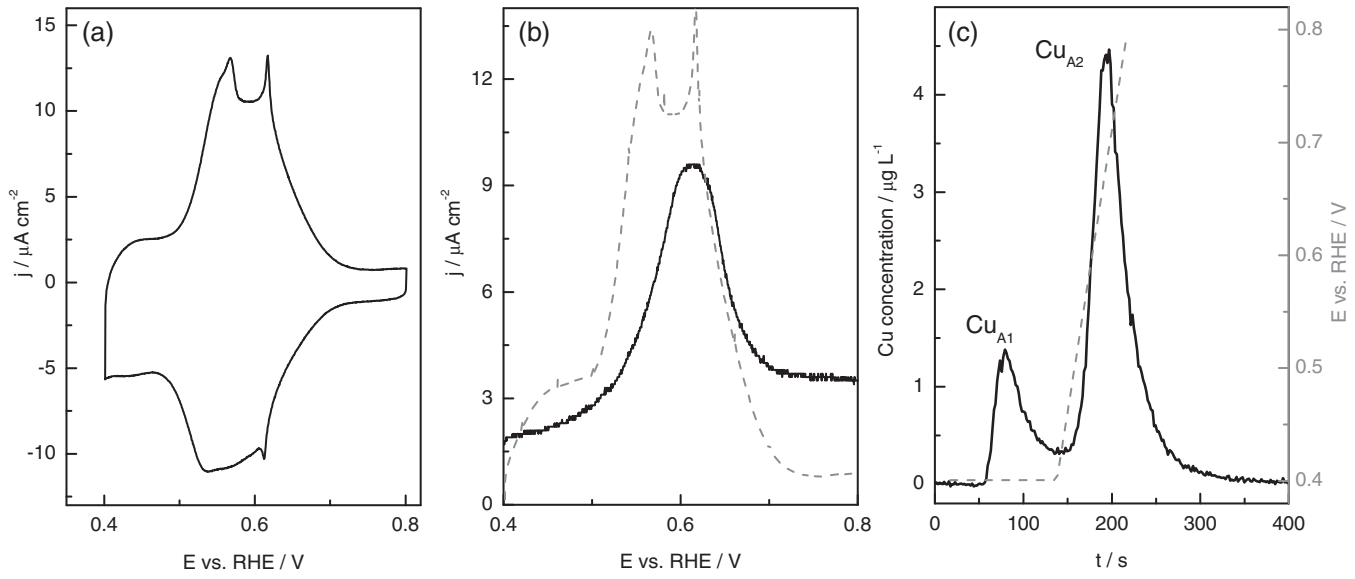

Figure 1. (a) Copper underpotential deposition/stripping cyclic voltammogram taken in a conventional three electrode cell with 0.1 M H_2SO_4 + 2.5 mM $CuSO_4$ as an electrolyte. (b) Copper stripping linear sweep voltammograms taken in a conventional three electrode cell with 0.1 M H_2SO_4 + 2.5 mM $CuSO_4$ as an electrolyte (dashed gray line) and in a scanning flow cell with 0.1 M $HClO_4$ electrolyte (solid line). (c) Copper dissolution mass-spectrogram. Dashed gray line shows applied potential program. Scan rate: 10 mV s^{-1}.

SFC. The charge was obtained by integrating the hydrogen desorption region of the CVs and subtracting the double layer capacitance measured by extrapolation from the double layer region. The obtained charge was ca. 51 ± 8 μC cm^{-2} for Pt@Au and ca. 270 μC cm^{-2} for Pt-poly. Using these numbers and taking into account the R_f of 1.3 and H_{UPD} charge on 1 cm^2 platinum surface of 210 μC cm^{-2}, θ_{Pt} was found to be 0.19 ± 0.03. A relatively high error is due to the difficulties in the integration of H_{UPD} related to the reduction of residual oxygen. This value is comparable but slightly lower than the maximal one. The observed discrepancy may be due to a non-ideal monolayer configuration. Comparing the θ_{Pt} values obtained from the two methods and assuming that there is formation of bilayers, it is found that a maximum of 30% of the Pt atoms can be in the second layer. By a similar argument, coverages for the third and subsequent layers will be significantly lower. It also cannot be ruled out that the charge of a Pt monolayer is different to 210 μC cm^{-2}, resulting in different coverages. In any case, our simple calculation shows that most of the deposited Pt is in the monolayer state. At some spots, however, multiple layers are possible. Their coverage, however, is relatively low. This conclusion is in line with those drawn for Pt deposition on Au(111).[25]

Platinum and gold transient and quasi-steady-state dissolution.—Dissolution of Pt@Au electrodes was studied by taking CVs at a relatively slow scan rate of 5 mV s^{-1}, so that details like anodic and cathodic dissolution are well-resolved on the resulting mass-spectrogram. A representative fragment of the mass-spectrogram of Au- and Pt-poly electrodes as well as Pt@Au electrodes showing dissolution of Au and Pt during excursion up to 1.5 V_{RHE} is shown in Figure 2a (see also Figure S2 in the ESI). The dissolution profiles of Au- and Pt-poly are similar to those previously reported.[23,24,31] Au predominantly dissolves anodically, while dissolution of Pt occurs mainly during reduction of the surface oxide, although anodic dissolution is still significant. Dissolution profiles of Au and Pt from the Pt@Au electrode are similar to that of Pt- and Au-poly. In particular, the onset potentials of anodic Pt and Au dissolution from Pt-poly and Au-poly and Pt@Au electrodes are comparable. Moreover, the onset stays virtually intact during 10 successive cycles. There are, however, important differences. First of all, anodic dissolution of both metals (especially Pt) is significantly suppressed, while there is only a minor change in the cathodic peak intensity. Secondly, there is also a change in the shape of the Pt dissolution profile. The appearance of an additional cathodic pre-peak is most likely due to Pt surface destabilization caused by Au oxide reduction.

Figure 2b shows the variation of the amount of Pt dissolved in anodic and cathodic peaks from Pt-poly and Pt@Au electrodes during successive potential cycles up to 1.5 V_{RHE}. Once again, the amount of dissolved Pt from both electrodes in the cathodic process is virtually the same, while the difference in anodically dissolved amounts is significant. This difference is quantified and presented in Figure 1c as the ratio between anodic and cathodic dissolution. The corresponding values for Pt-poly and Pt@Au are ca. 20 and 5%. In other words, anodic dissolution of Pt from Pt@Au is factor of four lower, which corresponds well to the reduced Pt coverage $\theta_{Pt} = 0.25$ and the notion that anodic dissolution of Pt is proportional to θ_{Pt}. On the other hand, cathodic dissolution is coverage-independent, which is equivalent to a four times larger θ_{Pt} normalized cathodic dissolution from the Pt@Au electrode.

It should be noted that in comparison to the behavior of the special Pt@Au system here, different ratios between anodic and cathodic peaks have been observed previously. For instance no anodic and increased cathodic dissolution was observed in CO-saturated electrolyte and the results were explained assuming healing of low-coordinated surface sites and suppressed re-deposition in the presence of CO.[32] Probably same reasoning can be used to explain an increased Pt dissolution in the presence of formic acid.[33] On the other hand, an enhanced anodic and suppressed cathodic dissolution have been observed at elevated temperatures.[23] Moreover, we have found that the ratio also

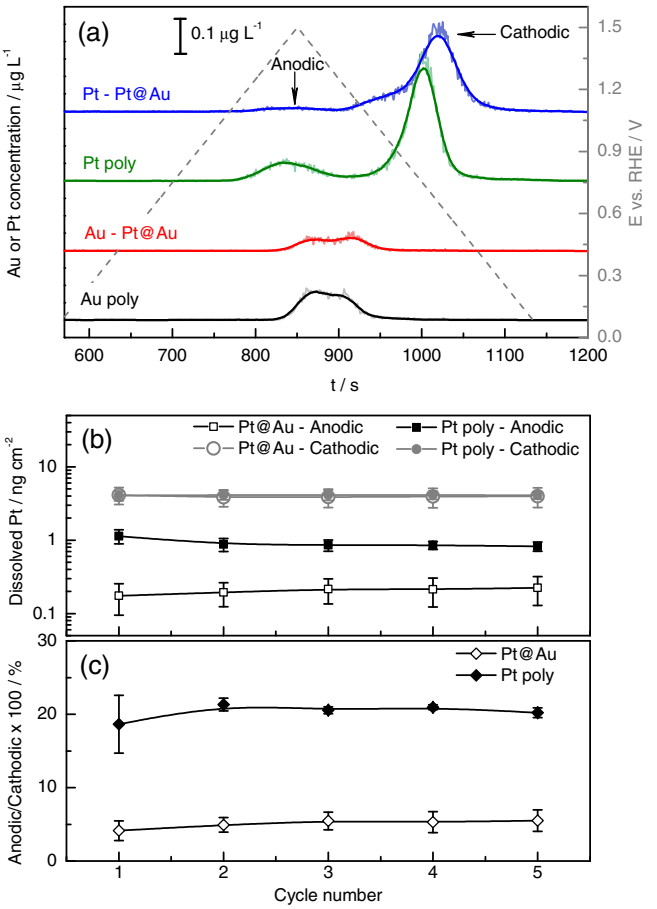

Figure 2. (a) Representative gold and platinum dissolution mass-spectrogram taken from polycrystalline platinum and gold electrodes, as well as submonolayer platinum covered gold electrodes, highlighting regions of anodic and cathodic dissolution. The dashed gray line indicates the applied potential program. (b) Change of platinum dissolution amount with number of cycles obtained by integration of corresponding anodic and cathodic dissolution peaks. (c) Ratio between anodic and cathodic dissolution represented as percentages.

depends on the applied supporting electrolyte. While a value of ca. 20% is typical for 0.1 M $HClO_4$, the ratio is ca. 5 – 10% (depending on the upper potential limit of cycles (E_{UPL})) in 0.1 M H_2SO_4 and 0.05 M NaOH,[31,34] also in accordance with results published by Pavlišič et al.[35]

To acquire information on the quasi-steady-state stability of Pt@Au, a 30 min polarization step at 1.0 V_{RHE} for accumulation and subsequent detection of dissolution products was used (more details on the employed experimental protocol can be found in Ref. 18). The resulting dissolution profile is shown in Figure 3. During 30 min at 1.0 V_{RHE} and a subsequent reductive ramp, the amount of dissolved Pt is 0.38 ± 0.06 and 0.22 ± 0.06 ng cm^{-2}, respectively (see inset in Figure 3). These values are at least one order of magnitude lower than that measured for transient dissolution. In comparison, the geometric surface area-normalized dissolution for a Pt-poly sample was 0.34 ± 0.1 and 0.14 ± 0.02 ng cm^{-2}, respectively. Hence, unlike in the transient dissolution experiments, the two sets of values are comparable. Normalized to θ_{Pt} Pt dissolution from the Pt@Au electrode is hence ca. 4 times higher.

Degradation of platinum sub-monolayer electrode during potential cycling.—Pt@Au or Pt alloy catalysts are usually reported to have a superior stability.[36,37] Indeed, if present as a small amount of adatoms occupying Pt surface defects Au seems to stabilize Pt toward dissolution, at least at low anodic potentials.[16,38,39] On the other hand,

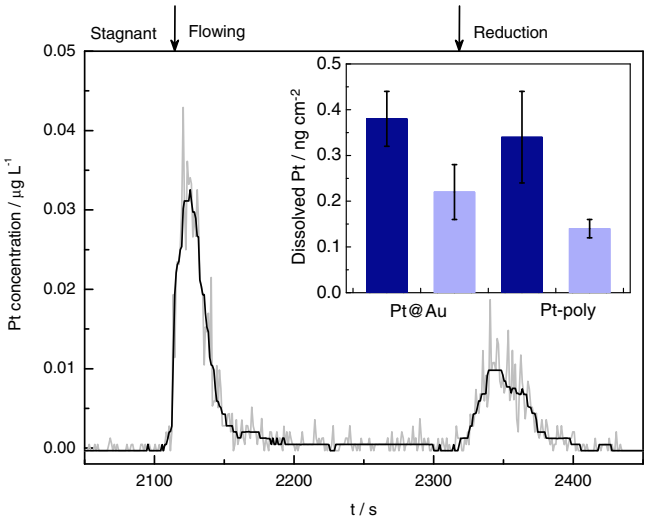

Figure 3. Quasi-steady-state dissolution of platinum. The electrode was held at E = 1.0 V_{RHE} over 30 min in a stagnant operational mode without electrolyte flow. Afterwards, the electrolyte flow was turned on to wash out platinum dissolution products. The second peak is due to platinum dissolution during the negative going potential ramp. Inset shows amounts of dissolved platinum from Pt@Au and Pt-poly electrodes in anodic (dark blue) and cathodic (light blue) processes, respectively.

due to a preference for Au surface segregation Pt@Au is predicted to be unstable.[40,41] It is not clear, however, how the Au surface segregation affects stability toward dissolution. As can be seen from Figures 2b, 2c during 5 cycles up to 1.5 V_{RHE} (or 10 as shown in Figure S3 in the ESI) there is virtually no change in the dissolution signal for both Pt and Pt@Au electrodes. On the other hand, the fact that Pt steadily dissolves means that θ_{Pt} must decrease and that at some point dissolution should drop simply due to material exhausting. To investigate this further, the experiments presented in Figure 2 were modified, viz. 30 degradation cycles at scan rate of 200 mV s^{-1} were added between each of the slow scans at 10 mV s^{-1}. Both slow and fast scans had the same E_{UPL} of 1.5 V_{RHE}. Figure 4a shows the corresponding dissolution profile for Pt and Au. Already over the first 30 degradation cycles a significant decrease in the dissolution signal appears. Afterwards the dissolution constantly drops with each new degradation step. It should be noted that in the same degradation protocol the dissolution signal from a Pt-poly electrode is stable (see Figure S4 in the ESI), which is not surprising considering the quasi-infinite Pt reservoir. CVs shown in Figure S5 in the ESI support this statement. Indeed, while there is virtually no change in H_{UPD} region for Pt-poly, it decreases drastically for Pt@Au.

The variation of Pt dissolution during anodic and cathodic dissolution, as well as during the accelerated degradation, with the number of cycles is shown in Figures 4b-4d, respectively. When the E_{UPL} of the degradation cycles is 1.1 V_{RHE} (the highest value typically adopted in accelerated degradation tests of core/shell catalysts), it can indeed be seen that the change in dissolution signal during the slow cycles to 1.5 V_{RHE} in between is marginal. The amount of anodically and cathodically dissolved Pt obtained by integration of 6 cycles at 10 mV s^{-1} up to 1.5 V_{RHE} is ca. 1.5 and 28.3 ng cm^{-2}, respectively. In comparison, the dissolution during the mild degradation accounts for ca. 4.2 ng cm^{-2}, which is ca. 3% of the initial Pt content of 130 ng cm^{-2}.

The situation changes drastically at E_{UPL} in the degradation cycles of 1.5 V_{RHE}. In this case, the amount of anodically and cathodically dissolved Pt in 6 cycles at 10 mV s^{-1} is ca. 0.8 and 15.4 ng cm^{-2}, respectively. The value is lower than that for degradation up to 1.1 V_{RHE}. The reason for the continuous decline is that the total dissolved Pt amount, including degradation cycles, amounts to ca. 110 ng cm^{-2}, closely approaching the total amount of Pt deposited on the Au

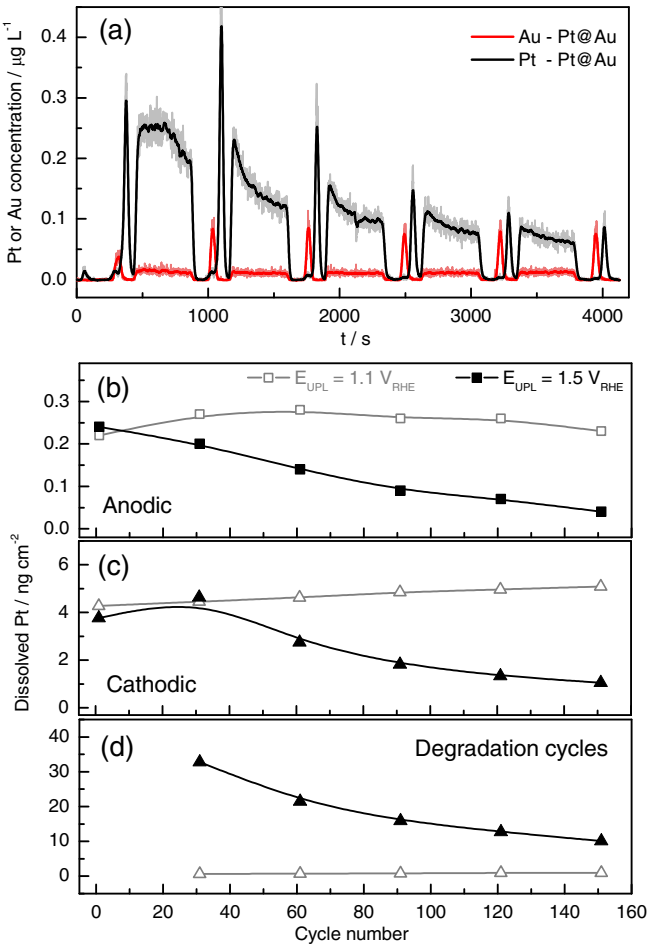

Figure 4. (a) Gold and platinum dissolution mass-spectrogram taken from sub-monolayer platinum supported on a gold electrode. Between each of the slow scans at 10 mV s^{-1}, 30 degradation cycles at 200 mV s^{-1} were applied in the accelerated degradation test. Corresponding variation of anodic and cathodic dissolution (b,c) and dissolution during degradation (d) with number of degradation cycles up to 1.1 (gray line) and 1.5 V_{RHE} (black line), respectively.

electrode. In parallel to the decrease in Pt content, the onset potential of anodic Pt dissolution shifts steadily from ca. 1.0 to 1.4 V_{RHE} during the slow scans, suggesting there is alloying and/or Au surface segregation.[42] The latter value corresponds to the onset of Au dissolution in 0.1 M $HClO_4$.[31] The dissolution rate at the end of the degradation cycles was ca. 24% of the rate at the beginning of the degradation protocol. This decrease, as well as the decrease in the cathodic dissolution in general, could be a sign of stabilization due to alloying, shifting the equilibrium concentration of dissolved Pt species to lower values. Alternatively, at such low coverages the equilibrium might not be established anymore in the given time interval, so that the observed lower dissolution values are now due to a kinetic limitation of dissolution. The total amount of dissolved Au for E_{UPL} = 1.5 V_{RHE} of ca. 15.5 ng cm^{-2} is also higher in comparison to cycles with E_{UPL} = 1.1 V_{RHE}. Au dissolution, however, does not show any significant variation with cycles. During degradation θ_{Au} changes from ca. θ_{Au} = 0.75 to 0.96 (see Figures S6 and S7 in the ESI). This result can be probably attributed to some stabilization effect of Pt on Au dissolution.

Discussion

We will limit our discussion to the case of Pt sub-monolayer dissolution, leaving the important and previously not addressed topic of underpotential deposition of Cu on Au studied by the novel

SFC-ICP-MS technique for a dedicated future study. The important result to be discussed first is the origin of the ratio change between the anodic and cathodic peak in transient dissolution experiments. The dependence of anodic dissolution on θ_{Pt} can be explained assuming that the process is far from equilibrium (concentration of dissolved species is lower than the equilibrium concentration at this potential) and dissolution is kinetically controlled. Slow dissolution can be related to sluggish kinetics of Pt oxidation, e.g. in an interfacial place-exchange process or any other mechanism in which oxygen from its adsorbed state moves into the lattice.[29,43] It seems that in the as-prepared Pt@Au samples the stabilizing effect (if any) of Au on sub-monolayer Pt is negligible. Otherwise, dissolution would not be proportional to coverage and a shift in the Pt dissolution onset potential would be expected. This result is in line with recent X-ray photoelectron spectroscopy (XPS) data on Pt sub-monolayers electrodeposited on Au substrate showing no significant change in the characteristic Pt XPS peaks shift in comparison to bulk Pt.[42]

The independence of cathodic dissolution from Pt coverage could be rationalized assuming a local saturation of dissolved Pt species close to the electrode preventing further dissolution. Hence, unlike anodic dissolution, cathodic dissolution is limited not by kinetics but by the establishment of equilibrium concentration of dissolved species and, hence, by mass transfer of dissolved species from the vicinity of the electrode. As there is no alloying (which would change the chemical potential of Pt) equilibrium potential/concentration for dissolved Pt ions in the vicinity of Pt-poly and Pt@Au should be similar. Cathodic dissolution must be a very fast process. Otherwise, dissolved products could diffuse out in the bulk electrolyte, preventing the establishment of equilibrium. In a recent work by Shrestha et al.[44] the authors suggested that cathodic dissolution of noble metals is triggered by an uncompensated positive charge that is built up temporarily in the oxide due to proton migration from the electrolyte into the oxide. Dissolution of metal ions compensates this charge imbalance. Alternatively, more facile kinetics of reverse place-exchange can be also suggested. Independent of the mechanism, reduction is much faster. All considered processes are comparably fast, which explains the observed experimental results of the current work.

Unlike in the fast anodic transient experiment, in the quasi-steady-state dissolution experiment the concentration of Pt close to the electrode is at or approaching equilibrium.[18] In this case the amount of dissolved material is controlled predominantly by the diffusion of dissolved species from the electrode to the bulk electrolyte, which must be comparable for both electrodes.

The situation is different for the cycled electrode. The decrease in the cathodic peak during degradation can be rationalized assuming formation of an alloy (or in general mixing) of Pt and Au, resulting in a shift in equilibrium concentration. Hence, there is some stabilization of Pt with Au at a relatively low θ_{Pt}. The observed shift in the Pt dissolution onset potential after potential cycling is clear evidence of such alloying between the metals. Alloying of Pt with Au during potential cycles was also suggested based on the XPS measurements.[42] Despite stabilization caused by alloying with Au, Pt dissolution is still significant and not proportional to the amount of Pt on the electrode. The excess in dissolution can be explained by dissolution triggered by Au oxide reduction. It is difficult to say with certainty if the measured cathodic dissolution in this case also represents the equilibrium concentration (lower due to alloying) or if the process comes to be controlled by kinetics.

At the moment there is no consensus in the literature regarding the exact electrochemical reactions behind the observed dissolution processes. Many reactions have been suggested. In our recent works several microscopic and macroscopic models of noble-metal dissolution have been proposed and discussed. In the microscopic model, an important destabilizing role of the interfacial place-exchange between the adsorbed O/OH groups and topmost layer of Pt or Au during oxide formation and a reverse process during oxide reduction were suggested.[29,34] Charge imbalance at the oxide/electrolyte interface due to fast proton consumption by oxide can be considered as an additional destabilizing factor during oxide reduction.[44] Macroscopically, several reactions were hypothesized. It is conceivable that there could exist an unstable short-lived intermediate (e.g. Au_2O and Pt_2O) of oxide formation/reduction which chemically or electrochemically dissolves.[31] Alternatively, it seems that early reported results can be explained by using two well-known dissolution reactions, namely direct electrochemical dissolution of metallic Pt and electrochemical dissolution of Pt dioxide (reactions 2 and 3 in Ref. 18, respectively).[45,46] Currently, we are working on a theoretical model of Pt dissolution which we hope will account for the experimentally collected data of the current and previous works.

In summary, the explanation suggested in the current work for transient and quasi-steady-state dissolution based on the kinetics of oxide formation and oxide reduction explains well the observed experimental results. It must be stated, however, that, as only one coverage has been studied, it is not clear if this conclusion can be transferred to other systems. In future works, we are going to address this issue by studying the effect of Pt coverage on Pt and Au dissolution, as well as the stability of other systems, especially Au@Pt suggested by Zhang et al.[39]

Conclusions

We will summarize the results of the current work in the light of application of Pt-based cathode catalysts in PEMFCs. The fact that in the quasi-steady-state dissolution experiments dissolved Pt amount does not depend on θ_{Pt} implies an enhanced real-surface-area-normalized dissolution with lower loadings, which is important to consider for PEMFC open circuit or low-current-density conditions. The same is true for transient cathodic dissolution, which occurs as the current density increases. Only the transient anodic dissolution scales directly with θ_{Pt}, so that the surface-area-normalized rate remains constant. The situation changes when Pt is alloyed with Au. In this case the equilibrium concentration is lower at a given potential, which should result in lower dissolution. It is not clear, however, if the reduced dissolution is due to a thermodynamic or a kinetic effect. Numerous core/shell systems have been suggested in the literature for the ORR, alcohol and formic acid oxidation, and other applications.[8,12,13,33] As in the case of Au-Pt, the stability of those systems is poorly understood. The results presented in the current work on the stability of Au-Pt can be already used for the prediction of platinum dissolution in other systems. Considering the minor stabilization of Pt toward dissolution by the presence of Au, the enhanced stability of high-surface-area catalysts reported previously in literature can be attributed most likely to a structural effect, e.g. the inhibition of support corrosion by the presence of Au at the catalyst/support interface. For a more fundamental understanding, however, further research on the effect of Pt coverage, of the degree of alloying, and of dissolution at lower potentials is necessary.

References

1. K. Sasaki, M. Shao, and R. Adzic, in *Polymer Electrolyte Fuel Cell Durability*, F. Büchi, M. Inaba, and T. Schmidt Editors, p. 7, Springer New York (2009).
2. S. S. Kocha, in *Polymer Electrolyte Fuel Cell Degradation*, M. M. Mench, E. C. Kumbur, and T. N. Veziroglu Editors, p. 89, Academic Press, Boston (2012).
3. D. J. Myers and X. Wang, in *Polymer Electrolyte Fuel Cells*, p. 153, Pan Stanford Publishing (2013).
4. P. Trogadas and T. F. Fuller, in *Polymer Electrolyte Membrane and Direct Methanol Fuel Cell Technology*, C. Hartnig and C. Roth Editors, p. 194, Woodhead Publishing (2012).
5. J. Zhang, *PEM Fuel Cell Electrocatalysts and Catalyst Layers: Fundamentals and Applications*, Springer-Verlag, London (2008).
6. O. Gröger, H. A. Gasteiger, and J.-P. Suchsland, *J. Electrochem. Soc.*, **162**, A2605 (2015).
7. M. Oezaslan, F. Hasché, and P. Strasser, *J. Phys. Chem. Lett.*, **4**, 3273 (2013).
8. R. R. Adzic, J. Zhang, K. Sasaki, M. B. Vukmirovic, M. Shao, J. X. Wang, A. U. Nilekar, M. Mavrikakis, J. A. Valerio, and F. Uribe, *Top. Catal.*, **46**, 249 (2007).
9. J. Zhang, M. B. Vukmirovic, Y. Xu, M. Mavrikakis, and R. R. Adzic, *Angew. Chem.*, **117**, 2170 (2005).
10. M. Shao, A. Peles, K. Shoemaker, M. Gummalla, P. N. Njoki, J. Luo, and C.-J. Zhong, *J. Phys. Chem. Lett.*, **2**, 67 (2011).
11. M. Shao, A. Peles, and J. Odell, *J. Phys. Chem. C*, **118**, 18505 (2014).

12. S. St. John, R. W. Atkinson, O. Dyck, C.-J. Sun, T. A. Zawodzinski, and A. B. Papandrew, *Chem. Commun.*, **51**, 16633 (2015).
13. N. Kristian, Y. Yan, and X. Wang, *Chem. Commun.*, 353 (2008).
14. Y. Kang, J. Snyder, M. Chi, D. Li, K. L. More, N. M. Markovic, and V. R. Stamenkovic, *Nano Lett.*, **14**, 6361 (2014).
15. C. Wang, D. van der Vliet, K. L. More, N. J. Zaluzec, S. Peng, S. Sun, H. Daimon, G. Wang, J. Greeley, J. Pearson, A. P. Paulikas, G. Karapetrov, D. Strmcnik, N. M. Markovic, and V. R. Stamenkovic, *Nano Lett.*, **11**, 919 (2011).
16. Y. Zhang, Q. Huang, Z. Zou, J. Yang, W. Vogel, and H. Yang, *J. Phys. Chem. C*, **114**, 6860 (2010).
17. S. Ball, in *Electrocatalysis in Fuel Cells*, M. Shao Editor, p. 561, Springer London (2013).
18. S. Cherevko, G. P. Keeley, S. Geiger, A. R. Zeradjanin, N. Hodnik, N. Kulyk, and K. J. J. Mayrhofer, *ChemElectroChem*, **2**, 1471 (2015).
19. Y. Furuya, T. Mashio, A. Ohma, M. Tian, F. Kaveh, D. Beauchemin, and G. Jerkiewicz, *ACS Catalysis*, **5**, 2605 (2015).
20. X. Wang, R. Kumar, and D. J. Myers, *Electrochem. Solid-State Lett.*, **9**, A225 (2006).
21. Z. Wang, E. Tada, and A. Nishikata, *Electrocatalysis*, **6**, 179 (2015).
22. S. G. Rinaldo, J. R. Stumper, and M. Eikerling, *J. Phys. Chem. C*, **114**, 5773 (2010).
23. S. Cherevko, A. A. Topalov, A. R. Zeradjanin, G. P. Keeley, and K. J. J. Mayrhofer, *Electrocatalysis*, **5**, 235 (2014).
24. S. Cherevko, A. R. Zeradjanin, A. A. Topalov, G. P. Keeley, and K. J. J. Mayrhofer, *J. Electrochem. Soc.*, **161**, H501 (2014).
25. S. R. Brankovic, J. X. Wang, and R. R. Adzic, *Surf. Sci.*, **474**, L173 (2001).
26. S. Ambrozik and N. Dimitrov, *Electrochim. Acta*, **169**, 248 (2015).
27. Y.-G. Kim, J. Y. Kim, D. Vairavapandian, and J. L. Stickney, *J. Phys. Chem. B*, **110**, 17998 (2006).
28. S. Cherevko, A. A. Topalov, I. Katsounaros, and K. J. J. Mayrhofer, *Electrochem. Commun.*, **28**, 44 (2013).
29. S. Cherevko, A. A. Topalov, A. R. Zeradjanin, I. Katsounaros, and K. J. J. Mayrhofer, *RSC Advances*, **3**, 16516 (2013).
30. H. Angerstein-Kozlowska, B. E. Conway, A. Hamelin, and L. Stoicoviciu, *J. Electroanal. Chem.*, **228**, 429 (1987).
31. S. Cherevko, A. R. Zeradjanin, G. P. Keeley, and K. J. J. Mayrhofer, *J. Electrochem. Soc.*, **161**, H822 (2014).
32. A. A. Topalov, A. R. Zeradjanin, S. Cherevko, and K. J. J. Mayrhofer, *Electrochem. Commun.*, **40**, 49 (2014).
33. M. Fayette, J. Nutariya, N. Vasiljevic, and N. Dimitrov, *ACS Catalysis*, **3**, 1709 (2013).
34. A. A. Topalov, S. Cherevko, A. Zeradjanin, J. Meier, I. Katsounaros, and K. J. J. Mayrhofer, *Chemical Science*, **5**, 631 (2014).
35. A. Pavlisic, P. Jovanovic, V. S. Selih, M. Sala, N. Hodnik, S. Hocevar, and M. Gaberscek, *Chem. Commun.*, **50**, 3732 (2014).
36. Y. Dai and S. Chen, *ACS Applied Materials & Interfaces*, **7**, 823 (2015).
37. D. Zhao and B.-Q. Xu, *Phys. Chem. Chem. Phys.*, **8**, 5106 (2006).
38. R. Jinnouchi, K. K. T. Suzuki, and Y. Morimoto, *Catal. Today*, **262**, 100 2016.
39. J. Zhang, K. Sasaki, E. Sutter, and R. R. Adzic, *Science*, **315**, 220 (2007).
40. G. Jerkiewicz, G. Vatankhah, J. Lessard, M. P. Soriaga, and Y.-S. Park, *Electrochim. Acta*, **49**, 1451 (2004).
41. F. Riccardo, *J. Phys.: Condens. Matter*, **27**, 013003 (2015).
42. S. H. Ahn, Y. Liu, and T. P. Moffat, *ACS Catalysis*, **5**, 2124 (2015).
43. G. Jerkiewicz, G. Vatankhah, J. Lessard, M. P. Soriaga, and Y.-S. Park, *Electrochim. Acta*, **49**, 1451 (2004).
44. B. R. Shrestha, T. Baimpos, S. Raman, and M. Valtiner, *ACS Nano*, **8**, 5979 (2014).
45. D. C. Johnson, D. T. Napp, and S. Bruckenstein, *Electrochim. Acta*, **15**, 1493 (1970).
46. D. A. J. Rand and R. Woods, *J. Electroanal. Chem.*, **35**, 209 (1972).